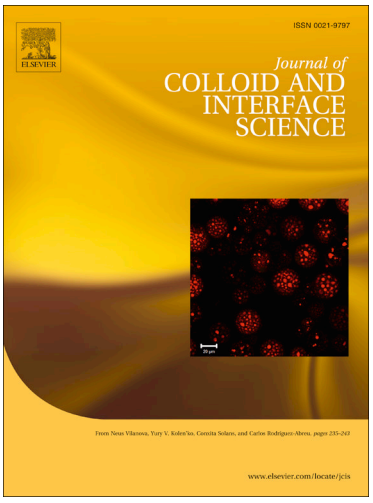

Construction of Sponge-like Graphitic Carbon Nitride and Silver Oxide Nanocomposite Probe for Highly Sensitive and Selective Turn-Off Fluorometric Detection of Hydrogen Peroxide

Aftab Ahmed, Akhtar Hayat, Mian Hasnain Nawaz, Peter John, Muhammad Nasir

PII: S0021-9797(19)31152-X
DOI: https://doi.org/10.1016/j.jcis.2019.09.109
Reference: YJCIS 25479

To appear in: *Journal of Colloid and Interface Science*

Received Date: 24 June 2019
Revised Date: 23 September 2019
Accepted Date: 27 September 2019

Please cite this article as: A. Ahmed, A. Hayat, M. Hasnain Nawaz, P. John, M. Nasir, Construction of Sponge-like Graphitic Carbon Nitride and Silver Oxide Nanocomposite Probe for Highly Sensitive and Selective Turn-Off Fluorometric Detection of Hydrogen Peroxide, *Journal of Colloid and Interface Science* (2019), doi: https://doi.org/10.1016/j.jcis.2019.09.109

Construction of Sponge-like Graphitic Carbon Nitride and Silver Oxide Nanocomposite Probe for Highly Sensitive and Selective Turn-Off Fluorometric Detection of Hydrogen Peroxide

Aftab Ahmed[1,2], Akhtar Hayat[1], Mian Hasnain Nawaz[1], Peter John[2*], Muhammad Nasir[1*]

[1] Interdisciplinary Research Centre in Biomedical Materials (IRCBM), COMSATS University Islamabad, Lahore Campus, 1.5 Km Defence Road, off Raiwind Road, Lahore, Punjab, Pakistan 54000

[2] Department of Chemistry, Government College University Lahore, Katchery Road, Anarkali, Lahore, Punjab, Pakistan 54000

*Corresponding Author: muhammadnasir@cuilahore.edu.pk (M. Nasir), peterjohn@gcu.edu.pk (P. John).

ABSTRACT

In the present work, spongy graphitic carbon nitride (GCN) and silver oxide nanocomposites were prepared through a facile hydrothermal method at 160^{o}C for 4h using GCN, silver nitrate, and dipotassium hydrogen phosphate as the starting materials. The prepared samples were characterized by scanning electron microscopy, energy dispersive X-ray spectrometry, Brunauer-Emmett-Teller method, X-ray diffraction, X-ray photoelectron spectroscopy (XPS), UV-Visible diffuse reflectance spectroscopy, Fourier transform infrared spectroscopy, Raman, and photoluminescence techniques. SEM images showed Ag_2O loaded GCN nanocomposite has a sponge-like structure due to the interconnecting of the enormous layer on the planar structure of GCN. XRD of samples showed the diffraction planes due to the hexagonal structure of carbon nitride with a decrease in intensity of peaks with increasing silver oxide (Ag_2O) in the nanocomposite. Further, the addition of silver oxide improved the electrical properties of the nanocomposite by reducing the recombination of electron and hole pairs as shown by photoluminescence spectra. XPS spectra have confirmed the oxidation state of Ag as well as the coexistence of Ag_2O and GCN in the nanocomposite. BET results indicated the increase in surface area for Ag_2O/GCN-4.2% nanocomposite as compared to GCN. FTIR study indicated that the graphitic structure in GCN remained intact with the loading of Ag_2O. A fluorescent quenching based H_2O_2 sensor was constructed by simultaneous oxidation of Rhodamine B in the presence of hydrogen peroxide and nanocomposite as the catalyst. In phosphate buffer saline at room temperature, Rhodamine B displayed a strong fluorescence emission peak around 577 nm under an excitation wavelength of 554 nm. This fluorescence signal of Rhodamine B was quenched in the presence of H_2O_2 and nanocomposite. The catalytic fluorescence quenching was increased with the increase in H_2O_2 concentration in the reaction system. The detection conditions of the prepared

sensor were optimized as a reaction temperature of 25^{o}C, Rhodamine B concentration as 66 ng mL^{-1} and nanocomposite concentration as 56 µg mL^{-1}. The catalytic fluorescence quenching response of the biosensor exhibited a linear range and limit of detection for H_2O_2 as 30 - 300 nM and 22 nM respectively.

KEYWORDS: Graphitic Carbon Nitride; Rhodamine B; H_2O_2; Fluorescence Quenching.

1. INTRODUCTION

Hydrogen peroxide (H_2O_2) is an important intermediate in the chemical and food industries. It also involved in biological and our life processes. [1] Its low concentration is used for signal transduction and expansion of the second messenger. Due to its bleaching, oxidizing and antiseptic properties, it is widely used in hair dyes, laundry detergent, and the propellant in rocketry, wastewater treatment, pharmaceuticals, food, cosmetics, horticulture, fish aeration, paper, and pulp industry. [2, 3] At high concentration, it is an aggressive oxidizer and corrode materials, causes an explosion upon contact with organic compounds. Toxicology study has linked oxidative stress, some physiological disorders, Alzheimer's neurodegenerative disorders and diabetes with its exposure. [4] It may also cause irritation to eyes, skin and mucous membranes, poisoning, respiratory inflammation, and hair bleaching in humans. Therefore, its accurate detection and determination are paramount important in realistic conditions. [5]

Various analytical techniques like high-performance liquid chromatography, electrochemical analysis, spectrophotometry, fluorescence spectroscopy, and chemiluminescence have been reported for the detection and determination of H_2O_2. [6] Among these sensing techniques, fluorescence [7] biosensing technique has gained special interest, and has been used in a variety of fields [8] for the estimation of the analyte. In the past, enzymatic fluorescence sensors were developed for the detection of H_2O_2. [9] However, enzymatic sensing strategy has suffered some limitations, such as high experiment cost, troublesome enzyme operations, and complicated modifications. Therefore, the development of fluorescence-off and non-enzymatic biosensing system was more reliable and suitable for the detection of an analyte.

The efficiency of catalytic fluorescence quenching biosensor is dependent upon the type and properties of nanomaterials. Graphitic-carbon-nitride (GCN) is a carbon-based, n-type

semiconductor. It is inexpensive and environmentally benign. [10, 11] It has a fascinating two-dimensional structure and consists of tri-s-triazine repeating units, which are bridged by nitrogen atoms. However, in recent decades, some properties such as poor electrical conductivity, the low surface to volume ratio and the high recombination rate of photogenerated electron-hole pairs have restricted its applications. To overcome these challenges, many efforts were reported for example improvement in synthesis method, nano-structuring, and functionalization with metal oxides [12] and so on. Herein, we have supported sponge-like GCN with metal oxide nanoparticles to promote the charge separations at the interface of semiconductor-metal heterojunction. This can further improve peroxidase-like-catalytic performance, enhancing selectivity and sensitivity of the product for sensing applications. [13]

Silver oxide (Ag_2O) is a p-type semiconductor. [14] Its nanoparticles are valuable and can be easily synthesized. Specific surface area, photoluminescence, and catalytic properties of Ag_2O nanoparticles are generally size-dependent. In aqueous solution, Ag_2O nanoparticles aggregate rapidly into micrometer-sized particles. That is why, well dispersion of nanoparticles with low agglomeration has remained a challenge in the synthesis process. To cope with this problem, Ag_2O nanoparticles can be supported on the surface of GCN. Because of the decoration of Ag_2O onto GCN, good interaction between the matrix and filler can be formed, which may reduce the agglomeration of the nanoparticle. Such nanocomposites have a large surface area and possessed better properties as compared to the simple nanomaterials. [15]

Herein, current work was an attempt to prepare a novel sponge-like biomimetic enzyme-free catalyst with high efficiency for H_2O_2 detection by utilizing self-assembling and interconnecting of the GCN skeleton and immobilizing Ag_2O nanoparticles onto the surface of GCN. The simple hydrothermal method was used to successfully synthesize sponge-like

Ag_2O/GCN nanocomposites. This sponge-like structure can be split into nanosheets by sonication. Characterization showed that GCN loaded Ag_2O has enhanced electrical properties, which was benefited for enhancement in the peroxidase-like activity of the catalyst. The fluorescence quenching of rhodamine B (RhB) was investigated in the presence and absence of the Ag_2O/GCN nanocomposite by H_2O_2. The Ag_2O/GCN-4.2% nanocomposite has demonstrated enhanced fluorescence quenching of RhB in the presence of H_2O_2 than those of the pristine GCN and other prepared Ag_2O/GCN nanocomposites. Based on this, a simple, low cost and non-enzymatic sensing platform for H_2O_2 detection were designed, which has high sensitivity and good selectivity.

2. MATERIALS AND METHODS

2.1. Materials and Reagents

Melamine ($C_3H_6N_6$), dipotassium hydrogen phosphate (K_2HPO_4), silver nitrate ($AgNO_3$), pyrocatechol, resorcinol, potassium chloride, sodium chloride, calcium chloride, hydrochloric acid, and sodium hydroxide were purchased from Sigma Aldrich. Rhodamine B was purchased from Avonchem. H_2O_2 (30%, w/v solution) and L-cysteine were received from Merck. Uric acid and D-glucose were received from BDH chemicals Ltd. L (+)-ascorbic acid was received from Daejung. Other chemicals and reagents were all analytical grade and used as received without further purification. All the solutions were prepared in PBS using ultra-pure water of conductivity less than 18 MΩ cm^{-1} obtained from Millipore system.

2.2. Instruments

The structure of the prepared samples was analyzed by X-ray powder diffraction (XRD) technique. XRD patterns were obtained using Rigaku D/max 2500 PC powder X-ray diffractometer. To analyze the surface morphology and shape of the prepared samples, the electron

microscope was used. Scanning electron microscope (SEM) images were taken on an electron microscope (Vega 3, LMU, and Tescan). Energy-dispersive X-ray spectrometry (EDX) was used to find the elemental composition and purity of samples. EDX was performed on the same SEM instrument. The Brunauer-Emmett-Teller (BET) specific surface area was determined by the BET method. The BET surface area measurements were done on a Micro-metrics ASAP-2020 (V 4.00-H) analyzer. The X-ray photoelectron spectroscopy (XPS) was used to find the chemical state and chemical environment of the elements in the samples. XPS determination was performed on an Axis-Ultra-Spectrometer system equipped with a mono-chromatized Aluminum metal, a Kα X-ray source of radiation (225 W). The high-resolution XPS spectra of C 1s, N 1s, O 1s, and Ag 3d regions were recorded. The possible functional groups in the samples were determined by using Fourier transform infrared (FTIR) spectroscopy. FTIR spectrum was collected on a FTIR spectrometer (Nicolet 6700, Thermo Fisher Scientific Instrument). UV-Visible diffusion reflectance spectroscopy (UV-Vis DRS) was used to determine the bandgap of semiconductor nanomaterial. UV-Vis DRS spectra of the samples were obtained by using Perkin Elmer Lambda 35 spectrophotometer. Raman spectroscopy was used to identify and study the chemical bonding and intramolecular bonds in the nanomaterial. Photoluminescence (PL) spectroscopy was used to probe the electronic structure of the nanomaterials. Raman and PL spectra were obtained with an InVia laser scanning confocal microscope (Renishaw, UK) with a laser excitation wavelength of 457 nm and an exposure time of 10 s at room temperature. UV-Vis absorption spectroscopy was used to determine the concentration of an analyte of interest. UV-Vis absorption spectra were obtained by using a UV-Vis absorption spectrophotometer (Perkin Elmer Lambda 25). Fluorescence spectroscopy was used to investigate the fluorescence properties of RhB and the

effect of analyte concentration on the fluorescence emission intensity of the dye. Fluorescence spectra were obtained on the Agilent Cary Eclipse fluorescence spectrophotometer (Varian, USA).

2.3. Synthesis of Graphitic Carbon Nitride

The GCN was prepared by the calcination method as cited [16] with minor modifications. Briefly, 15 gm of melamine powder was put into the ceramic boats and heated in the muffle furnace under the static air condition with a final temperature of 550^{o}C and a ramp rate of 5^{o}C min^{-1} for 4h. After calcination, the furnace was cooled naturally, and the pale-yellow powder was obtained, which was grounded to a fine powder with mortar and pestle.

2.4. Synthesis of Ag_2O/GCN Nanocomposites

The Ag_2O/GCN nanocomposites were prepared through the hydrothermal method. Typically, 250 mg of bulk GCN and 0, 8.2, 19.1, 31, 62 mg of $AgNO_3$ were added in 40 mL of the distilled water and sonicated for 10 minutes. After the adsorption of silver (Ag) ions on GCN suspension, 0, 6, 13, 21, 42 mg of K_2HPO_4 were added to the reaction mixture and heated up to 80^{o}C, so that silver was changed to silver phosphate (Ag_3PO_4).

$$3AgNO_3 + 2K_2HPO_4 \xrightarrow{80°C} Ag_3PO_4 + 3KNO_3 + KH_2PO_4$$

Then, the reaction mixture containing GCN and Ag_3PO_4 was hydrothermally treated at 160^{o}C for 4h. After the completion of the heating process, the cooling cycle was performed under the normal temperature and pressure conditions. The obtained mixture was centrifuged, the supernatant was discarded and subsequently washed several times with the distilled water. The resultant samples were dried at 60^{o}C for 24h in a drying oven. The prepared Ag_2O/GCN nanocomposites were contained 0, 2.1, 4.2, 8.4, and 16.8 percent of Ag_2O with respect to a constant

amount of GCN, which were denoted as GCN, Ag_2O/GCN-2.1%, Ag_2O/GCN-4.2%, Ag_2O/GCN-8.4%, and Ag_2O/GCN-16.8% respectively.

2.5. Fluorescent and Colorimetric Analysis

Stock suspensions of the samples were prepared by dispersing 5 mg of each sample in 2 mL of the distilled water followed by water-bath sonication at 40^{o}C for 10 minutes. RhB stock solution was prepared by dissolving 0.5 mg of the dye in 10 mL of the PBS. Then, diluting 67 µL of the dye solution to 50 mL using PBS. The final concentration of the stock dye was 67 ng mL^{-1}. Similarly, a stock 1 mM H_2O_2 was prepared. First, 10 mM H_2O_2 was prepared by diluting 1µL of 30% H_2O_2 to 1000 µL with the distilled water. Then, 500 µL of 10 mM was diluted to 5000 µL to prepare a stock 1 mM H_2O_2 solution. Every time a fresh dye and fresh H_2O_2 solutions were taken for recording the spectra.

In a typical procedure, 89.8 µL of stock nanocomposite suspension was added into 3909 µL of the stock dye solution followed by ultrasonication for 10 minutes and incubation for 1h to establish an equilibrium. Recorded the fluorescence emission spectra under an excitation wavelength of 554 nm to determine the fluorescence intensity of reaction mixture at 557 nm (F_o). Then, 1.2 µL of H_2O_2 (1 mM) was added, incubated the reaction mixture for 10 min and again fluorescence emission spectra were recorded to determine fluorescence intensity at 577 nm (F_{577}). Then, the catalytic fluorescence quenching ($\Delta F_{577\,\mathrm{nm}} = F_o - F_{577}$) was calculated. For colorimetric analysis, a reagent blank containing only dye and H_2O_2 was prepared and its absorbance at 554 nm (A_o) was recorded. Then, absorbance at 554 nm of the reaction mixture containing dye, nanocomposite, and H_2O_2 was recorded (A_{554} nm). The difference between both the absorbance ($\Delta A_{577\,\mathrm{nm}} = A_o - A_{577}$) gave the catalytic absorbance quenching by H_2O_2. The

final concentration of dye, nanocomposite, and H_2O_2 were 66 ng mL^{-1}, 56 µg mL^{-1} and 300 nM in the reaction mixture respectively.

3. RESULTS AND DISCUSSIONS

3.1. Detection Strategies

The electron transfer process in the nanocomposite structure and fluorescence quenching process of the Ag_2O/GCN-RhmB system by H_2O_2 were shown in Scheme 1. Ag_2O has a narrow bandgap of 1.2 eV, its conduction/valence band is lower than those of the GCN. GCN has a high electron and hole recombination rate, which was the main reason for its low catalytic activity. In our prepared nanocomposite system, photogenerated electrons on the conduction band of GCN may be easily transferred to the conduction band of Ag_2O, leading to the separation of electron-hole pairs in the nanocomposite. [17] The addition of nanocomposite in RhB solution has resulted in the deposition of dye on the nanocomposite surface and fluorescence signal of dye was decreased. This reaction system was used for H_2O_2 detection. The addition of H_2O_2 in this reaction system has resulted in the formation of hydroxyl radicals (•OH) and ions by the effect of Nano-catalyst, which could further oxidize the RhB. As a result, the fluorescence signal of the RhB was further quenched and fluorescence quenching at this stage was proportional to H_2O_2 concentration. Based on the oxidation of RhB by •OH radicals, a possible mechanism of the reaction was proposed and described in the following reaction equations.

$$Ag_2O/GCN + h\upsilon \rightarrow Ag_2O/GCN\ (e^- + h^+)$$

$$Ag_2O/GCN(e^-) + H_2O_2 \rightarrow OH^\bullet + OH^-$$

$$Ag_2O/GCN(h^+) + H_2O \rightarrow OH^\bullet + H^+$$

$$OH^\bullet + RhB \rightarrow CO_2 + H_2$$

$2H^+ + 2OH^- \rightarrow 2H_2O$

$h^+ + e^- \rightarrow (e^- + h^+)$ Negligible Recombination Reaction

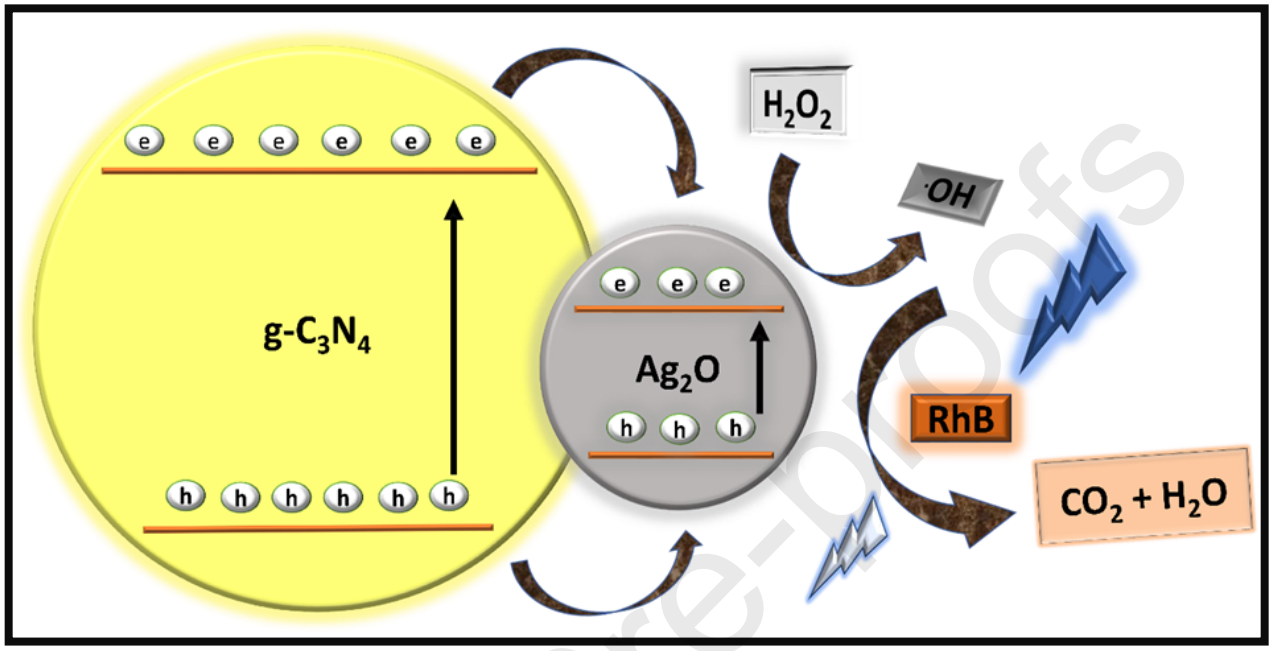

Scheme 1. The principle of fluorescence quenching biosensor for the detection of H_2O_2.

3.2. Characterizations of Proposed Biosensor

SEM images of the prepared samples are shown in Fig. 1. GCN showed a sponge-type structure consists of GCN nanosheets. In this sponge-like structure, nanosheets were self-assembled into porous, highly interconnected in isotropic configuration to form a 3D framework. On the surface of the sponge-like structure, planar objects evidenced the enormous layers or clusters of GCN sheets. The growth process of sponge-like structure can also be the result of penetration and consecutive staking of numerous GCN nanosheets into micrometer thick layers. In the nanocomposites, Ag_2O was distributed over the two-dimensional surface of GCN. The addition of the silver oxide nanoparticles in the GCN structure was happened to affect the sponge-like structure of the GCN. This is evident from the SEM of Ag_2O/GCN-4.2% nanocomposite,

which shows distorted and brittle sheets of GCN as compared to the sample without silver oxide. Further increase in the silver oxide concentration in the GCN destroyed the sponge-like structure of GCN as can be seen in Ag_2O/GCN-8.4% nanocomposite.

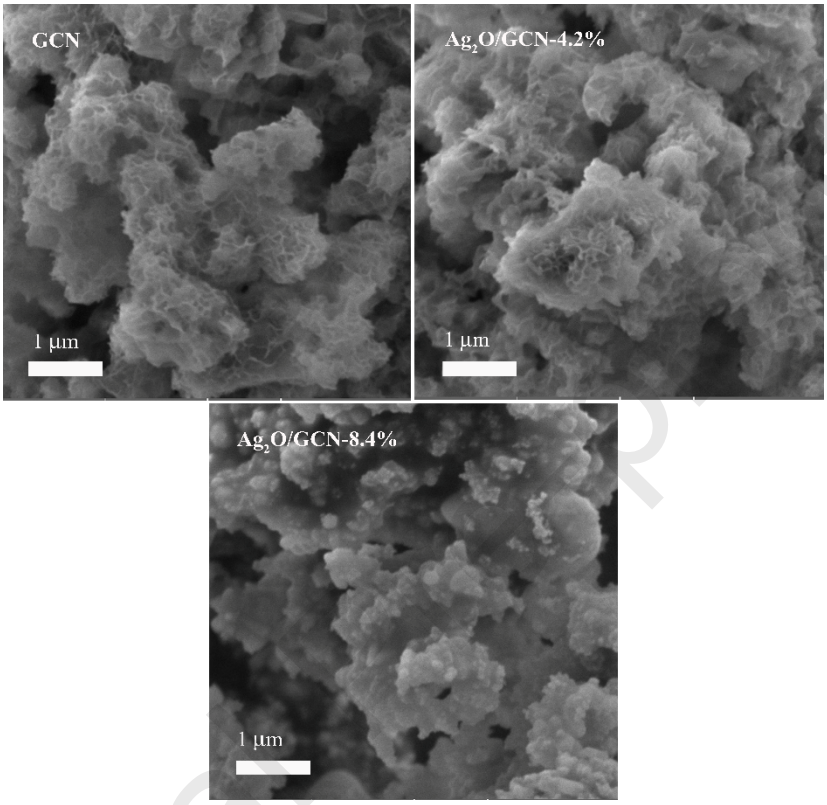

Fig. 1. SEM images of prepared GCN and Ag_2O/GCN nanocomposites.

The EDX spectra of GCN and Ag_2O/GCN nanocomposites were shown in Fig. 2. EDX results have confirmed the co-existence of both Ag_2O and GCN in the prepared nanocomposite. The EDX peaks were corresponding to the C, N, O and Ag atoms in the nanocomposite spectrum, whereas in GCN spectrum peaks were corresponding to the C and N atoms only. Moreover, there were no impurities peaks were found in the spectrum of the prepared samples.

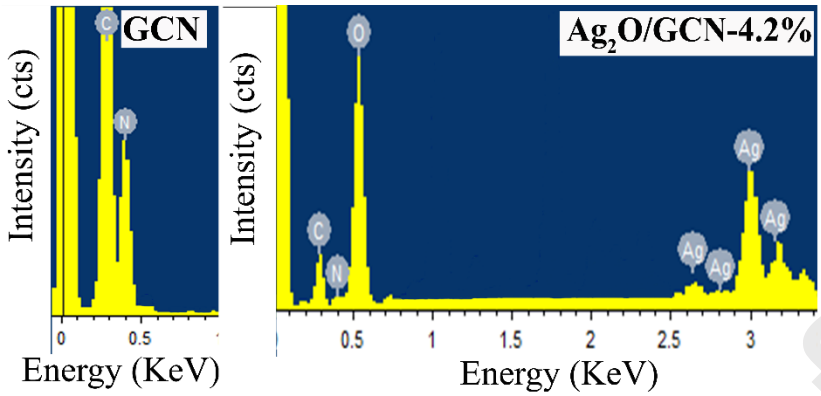

Fig. 2. EDX spectra of GCN and Ag_2O/GCN nanocomposites.

A comparison of weight (%) and atomic (%) of different elements present in samples were shown in Table 1. The C/N ratio of GCN was calculated as 0.69 and it was lower than the theoretical value of 0.75, which was due to the presence of uncondensed -NH_2 groups. A high percentage of O and C in the C/N ratio were observed for Ag_2O/GCN-4.2%, which was considered due to the presence of carbon dioxide in the pores of the sample, involvement of C from the laser beam and from the double adhesive tape.

Table 1. Chemical compositions according to EDX result

Samples	**Wt %**				**Atomic%**			
Elements	**C**	**N**	**O**	**Ag**	**C**	**N**	**O**	**Ag**
GCN	41	59	-	-	45	55	-	-
Ag_2O/GCN-4.2%	8	7	79	6	11	6	82	1

N_2 adsorption measurement was performed to study the surface area of GCN and Ag_2O/GCN nanocomposites and shown in Fig. 3. The surface area of Ag_2O/GCN-4.2% nanocomposite was calculated by using the BET method as 26.13 $m^2 \cdot g^{-1}$, which was much higher than that of the GCN (8.24 $m^2 \cdot g^{-1}$). This could be due to the lowering particle size after the incorporation of silver oxide in graphitic carbon nitride nanostructure.

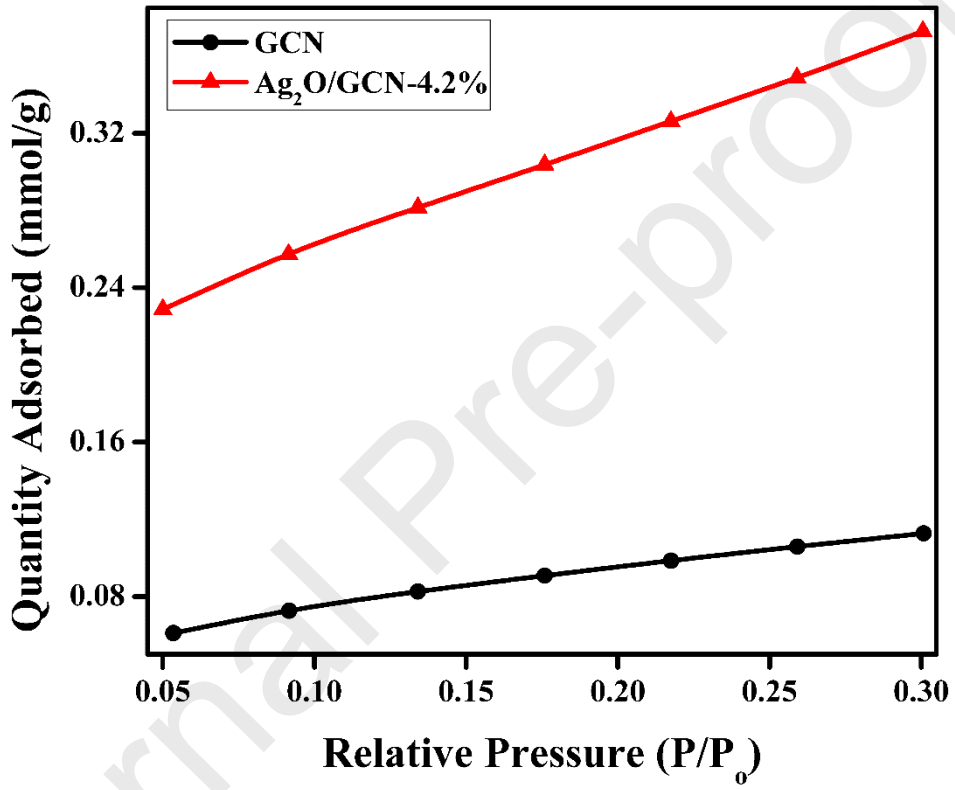

Fig. 3. BET spectra of GCN and Ag_2O/GCN nanocomposites.

XRD patterns of samples were shown in Fig. 4. The GCN spectrum has shown two diffraction peaks at 13.3° and 27.5°, which were indexed to (100) and (002) diffraction planes of the hexagonal GCN (JCPDS 87-1526) respectively. The first peak was the characteristics of interplanar staking of the aromatic system, whereas the second peak was the characteristics of inter-layer structural packing. [18] In nanocomposites, the intensity of both peaks was decreased with the increase in the percentage of Ag_2O. Some peaks in nanocomposites for Ag_2O were found

at 26.7, 31.5, 55.1, 63.1, and 69°, which were indexed to (110), (111), (220), (311) and (222) diffraction planes of Ag_2O phase (JCPDS 41-1104). These findings showed that nanocomposites contain both GCN and Ag_2O phases. There were no impurity peaks observed in the spectrum of the nanocomposite. The pure GCN spectrum shows a more amorphous nature as compared to the nanocomposites. These results indicated the coexistence of Ag_2O and GCN in nanocomposites.

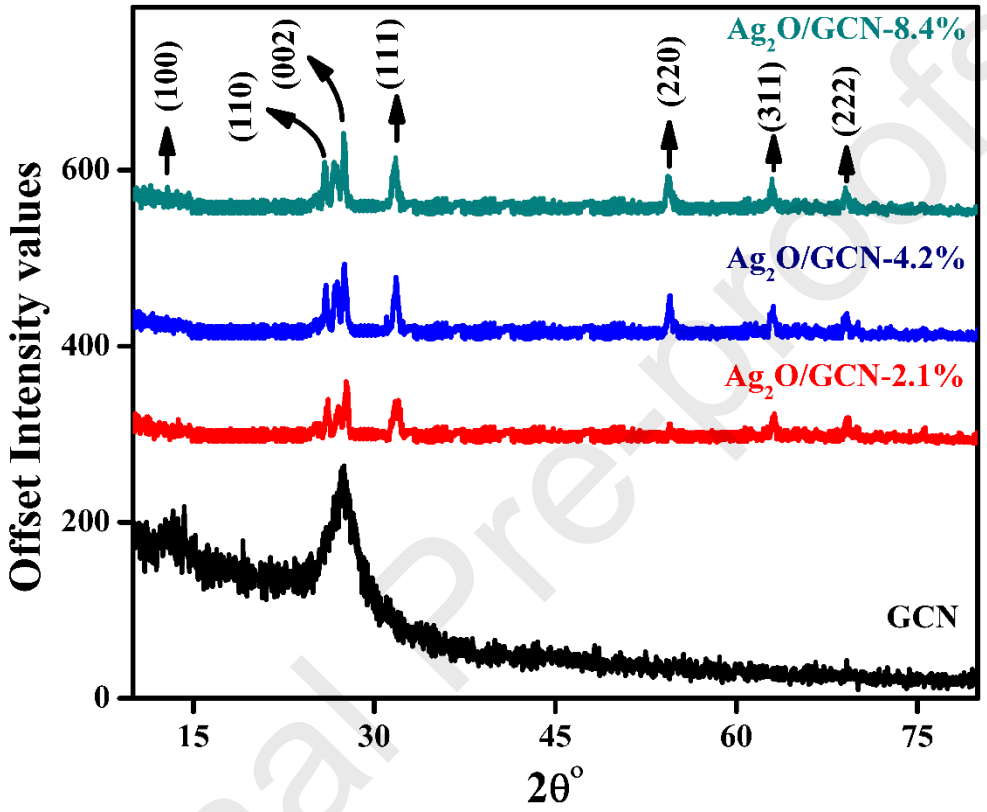

Fig. 4. XRD patterns of GCN and Ag_2O/GCN nanocomposites.

The composition of the prepared samples was determined through XPS analysis. Presence of different Gaussian-Lorentzian peaks in the typical high-resolution XPS spectra of C 1s, N 1s, O 1s, and Ag 3d was determined through peak deconvolution and shown in Fig. 3. Fig. 5B shows the deconvoluted C1s spectrum of the GCN and nanocomposite. The peak centered at 284.8 eV can be attributed to the surface adventitious C−C coordination, whereas the peak centered at 288.5 eV in GCN and 288.6 eV in nanocomposite corresponded to sp^2-bonded C atoms having N−C=N

coordination in the pure graphitic site in the aromatic ring. [19] The peak at 285.6 eV in GCN and 285.7 eV in nanocomposite was assigned to the sp^3-hybridized C atoms in CN and sp^2-hybridized C atoms in the aromatic ring bonded with NH_2 functional group. [19] [20] It was found that the composite C 1s peaks (C−N=C and CN) have high binding energy as compare to the binding energy of GCN peaks. The N 1s peak in the XPS spectrum was deconvoluted into four Gaussian-Lorentzian peaks as shown in Fig. 5C. The peak at 398.6 eV in GCN and 398.7 eV in nanocomposite was attributed to the pyridinic-like-nitrogen atoms bonded to two carbon atoms ($N-sp^2C$). Peaks at 399.4 and 400.1 eV in the GCN and nanocomposite was assigned to the graphitic-tertiary-nitrogen ($N-(C)_3$) atoms. Similarly, peaks at 401.7 and 401.2 eV in the GCN and nanocomposite was ascribed to C−N−H bonded N atoms. [19] [20] The fourth peak at 404.7 and 404.5 eV in CN and nanocomposite was considered due to the charging effects. The C−N=C and tertiary nitrogen atoms peaks were shifted to higher binding energy for nanocomposite. This small shift in the C 1s and N 1s peaks between GCN and Ag_2O/GCN-4.2% nanocomposite represented a strong interaction between GCN and Ag_2O at the heterojunction interface. [21] Ag 3d and O 1s deconvoluted peaks of the nanocomposite are shown in Fig.5D. The doublet peak of Ag 3d located at 368.6 and 374.7 eV was assigned to the Ag^+ $3d_{5/2}$ and Ag^+ $3d_{3/2}$ respectively. Similarly, O 1sis deconvoluted into two with the peaks at 529.6 and 531.6 eV, which the presence of O atoms in the lattice of Ag_2O nanoparticles. [22] Furthermore, the binding energy values of N 1s and Ag 3d in the composite was slightly higher than those of the GCN and the reported valued of pure Ag_2O. This shift in binding energy values was ascribed to the existence of a strong interaction between sponge-like GCN and Ag_2O nanoparticles.

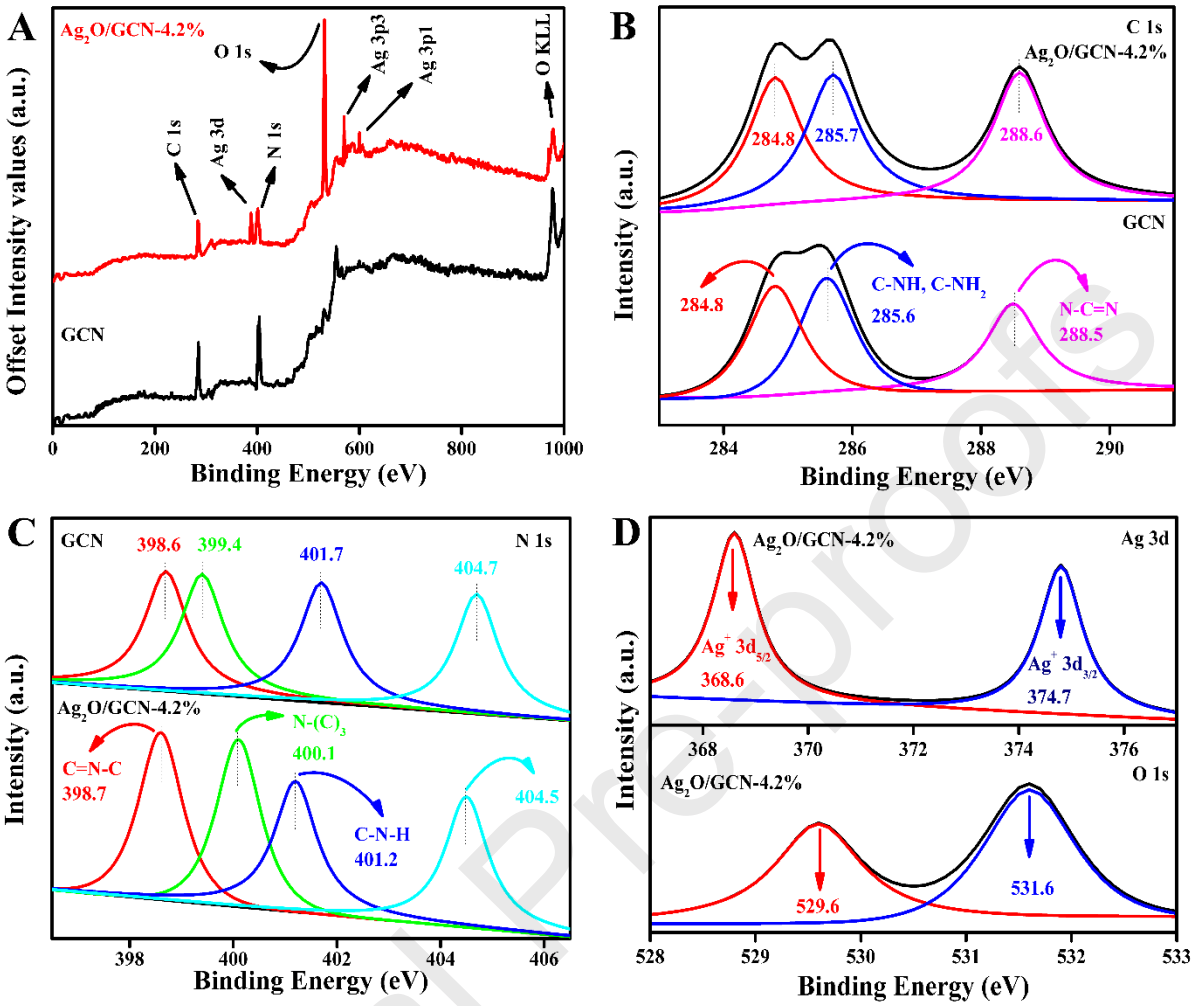

Fig. 5. (A) XPS survey, (B–D) Deconvoluted C1s, N1s, and O1s and Ag 3d XPS spectra of the prepared samples.

The optical properties of GCN and Ag_2O/GCN nanocomposites were investigated by using UV-Vis DRS. As shown in Fig. 6, the absorption pattern of GCN was similar to a typical carbon nitride-based organic semiconductor with a strong absorption around 430 nm. The loading of Ag_2O on GCN has significantly altered the optical absorption response of nanocomposites and the absorption intensity of composites gradually increased as the amount of Ag_2O nanoparticles increased. Therefore, increasing the loading of Ag_2O in the nanocomposites was resulted in the

redshift in the absorption intensity as compared to GCN in the whole visible-light range. This enhancement in light absorption intensity could be led to the production of more photo-induced electrons-hole pairs, which has resulted in the enhancement of the peroxidase-like activity of nanocomposites as compared to pure GCN. These findings also indicated an effective surface hybridization and an interaction between the Ag_2O nanoparticles and sponge-like GCN nanosheets in the nanocomposite system. The Tauc plot for GCN, Ag_2O/GCN-2.1%, and Ag_2O/GCN-4.2% was obtained by plotting $(\alpha h\nu)^{1/2}$ versus energy ($h\nu$) in electron volts (eV) and shown in the inset graph of Fig. 6. The bandgap energy was calculated by the intersection of tangent lines and horizontal axis as shown in the dotted lines in the inset graph of Fig.6. The bandgap of GCN, Ag_2O/GCN-2.1%, and Ag_2O/GCN-4.2% nanocomposites was calculated as 2.89, 2.80 and 2.43 eV respectively. As compared to GCN, the bandgap energy of Ag_2O/GCN-4.2% is small, which indicated an easier trend for the Ag_2O/GCN-4.2% to produce the electron-hole pairs through the absorption of the wavelength of the light. [23] These shifts also indicated the formation of heterojunction between Ag_2O and GCN, which have significantly improved the optical properties of the products.

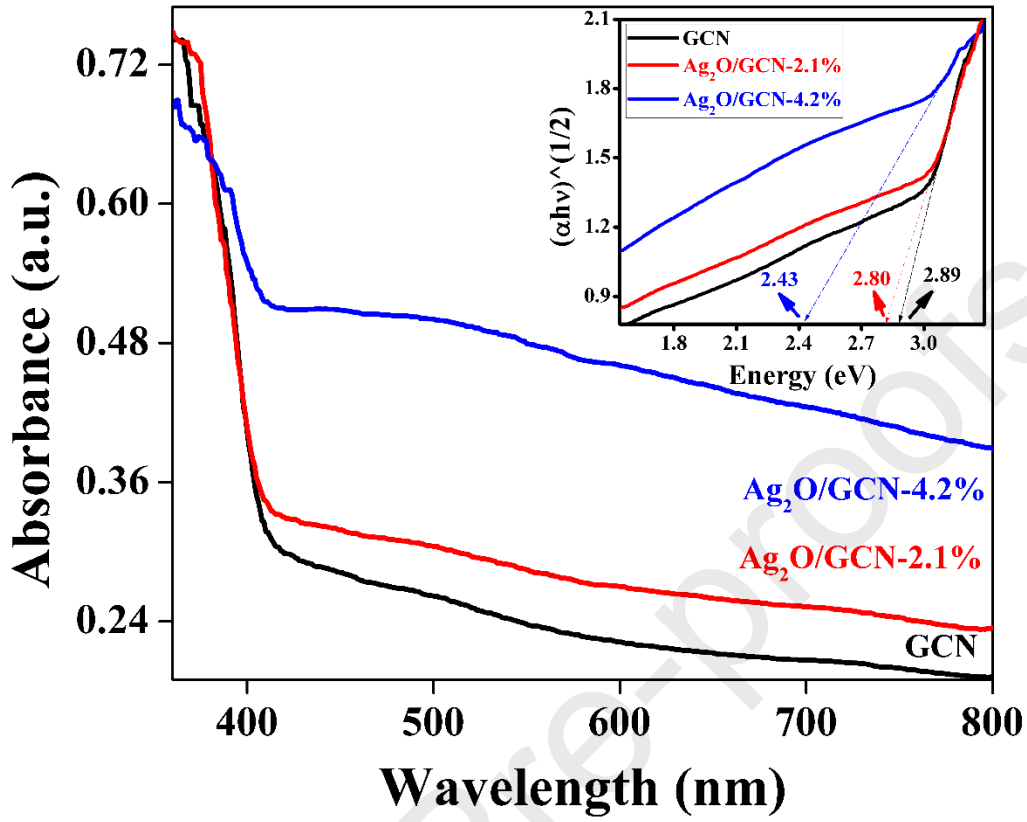

Fig. 6. UV-Vis DRS spectra of GCN and Ag_2O/GCN nanocomposites. The inset graph shows the $(\alpha h\nu)^{1/2}$ versus energy curves of the as-prepared GCN, Ag_2O/GCN-2.1%, and Ag_2O/GCN-4.2% samples.

The FTIR spectra of the samples were shown in Fig. 7. For GCN, a broad peak at 3000 - 3700 cm^{-1} was assigned to the stretching vibration of O-H of the physically adsorbed water molecules and the stretching vibration of N−H. [24] The absorbance intensity and broadness of 3000 - 3700 cm^{-1} bands and peak around 1600 cm^{-1} were enhanced as the percentage of Ag_2O was increased and became more prominent for Ag_2O/GCN-16.8% nanocomposite. This was attributed to the presence of more hydroxyl groups and an increased in the physical adsorption of water molecules with the increase of Ag_2O on the surface of sponge-like GCN in the nanocomposites.

The peak at 2360 cm^{-1} was attributed to the C=O functional group of carbon dioxide in the samples. The strong-band in the range of 1300 - 1700 cm^{-1} was assigned to the typical stretching vibration of CN heterocycles of sponge-like GCN in the samples. A sharp peak can be seen in the range of 810 - 1250 cm^{-1} for GCN and nanocomposites and was attributed to the breathing-mode of triazine-units and out-of-plane C-H bonds in the aromatic domain. In nanocomposites, an increase in sharpness and an increase in the intensity of this peak was observed, which was related to the increase of Ag_2O loading and reached maximum for Ag_2O/GCN-4.2%, further loading of Ag_2O has resulted in the decrease in intensity and increase in the broadness of this peak. This can be considered that the surface functional groups of sponge-like GCN were not affected too much till the loading of Ag_2O was 4.2 percent but further increase in its amount has resulted in the masking of more surface functional groups of GCN and distortion of its sponge-like structure as well as an agglomeration of Ag_2O has occurred. Based on the above observations, it was confirmed that Ag_2O/GCN-4.2% nanocomposites have close interfacial contact between Ag_2O and sponge-like GCN. This contact between Ag_2O and GCN was served as an electron migration path to enhance charge separation and induced a synergistic effect to further facilitate the efficient detection of H_2O_2.

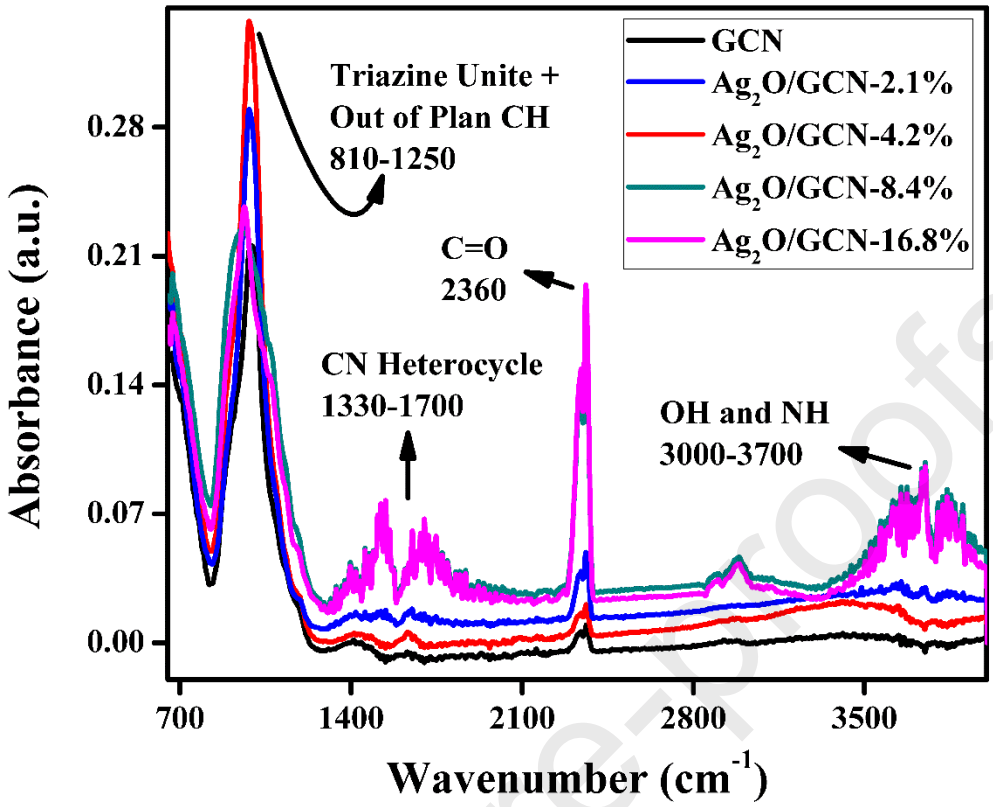

Fig. 7. FTIR spectra of GCN and Ag_2O/GCN nanocomposites.

The surface phase of synthesized samples was analyzed by Raman spectroscopy. [25] [26] As can be seen in Fig. 8, GCN spectra has shown several characteristics peaks, a strong peak at 667 cm^{-1} with a broad shoulder in the range of 520-930 cm^{-1} was related to vibration of the s-triazine ring inside GCN phase and relatively less intensive peaks were appeared at 178, 1300 (D peak) and 1607 cm^{-1} (G peak). In the case of Ag_2O/GCN composites, relative intensive peaks of Ag_2O at 248 and 430 cm^{-1} were appeared, which indicated that the second phase on the surface of composite was Ag_2O. The main peak at 667 cm^{-1} of GCN was split into two peaks and the intensity of main peaks at 178 and 667 cm^{-1} was suppressed. Several new peaks were observed in 1920, 1260 and 990 cm^{-1}. These variations in spectra indicated the interaction and interfacial contact between Ag_2O and GCN in composites, which was beneficial to prolong separation between

photogenerated electron-hole pairs. Raman results showed that GCN and Ag_2O were successfully coupled together.

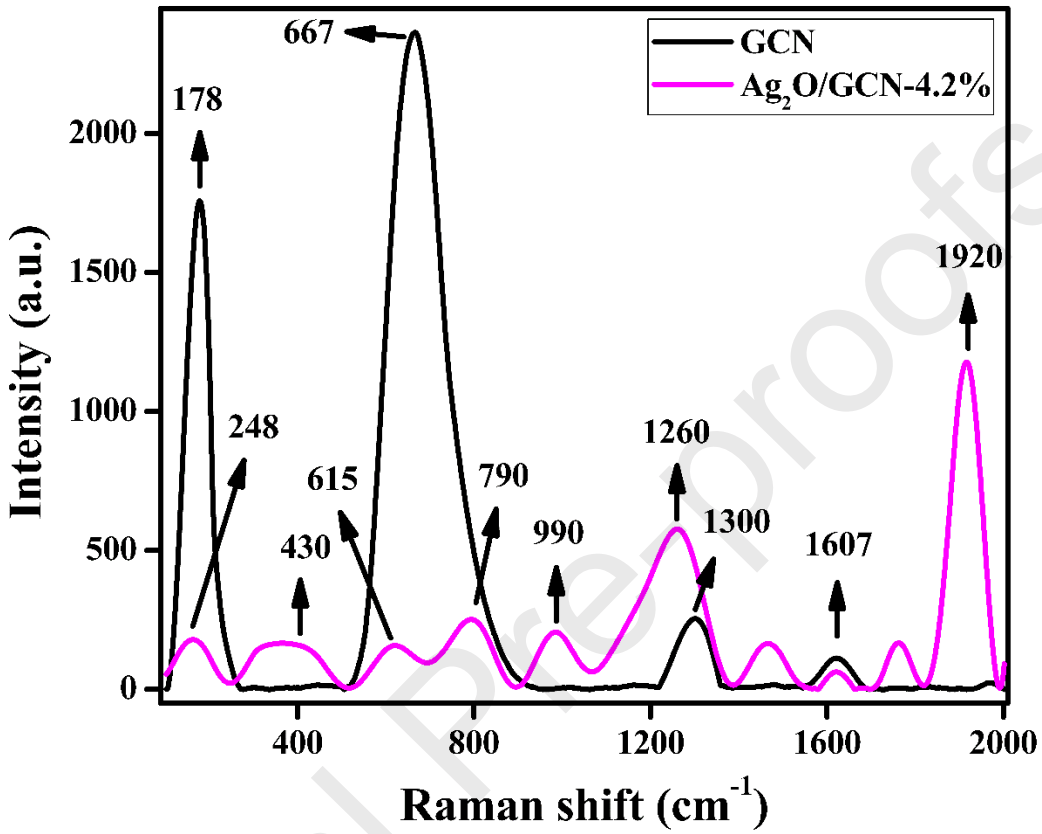

Fig. 8. Raman spectra of GCN and Ag_2O/GCN composites.

PL spectroscopy was used to investigate the recombination, transfer, and migration of the photogenerated charge carriers in a semiconductor. [12] PL spectra of the pure sponge-like GCN and Ag_2O/GCN nanocomposites at an excitation of 457 nm and at room temperature were shown in Fig. 9. All the samples exhibited an emission peak around 665 nm. The PL intensity of this main emission peak was significantly weakened with the increase in the percentage of Ag_2O in the nanocomposite. This variation in the PL spectra of nanocomposites was attributed to the efficient charge transfer and lowering of the recombination of photogenerated electron-hole pairs at the

heterojunction between Ag_2O and GCN, which has increased the separation of the photogenerated charge carriers. These results were well consistent with the experimental finding of the biosensor.

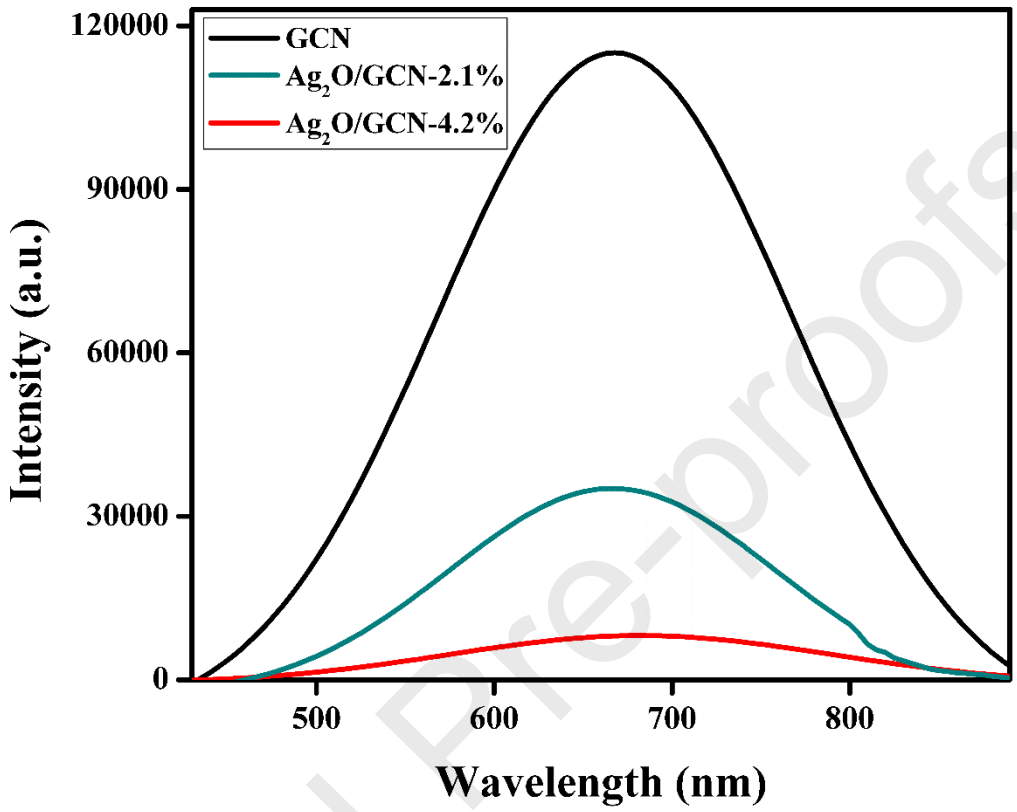

Fig. 9. PL spectra of the GCN and Ag_2O/GCN nanocomposites.

3.3. Optimization of the Reaction Conditions

A pre-scan spectrum of RhB (66 ng mL^{-1}) solution was recorded in the range of 200 - 800 nm and was shown in Fig. 10A. RhB solution exhibited a strong excitation peak at 554 nm and a corresponding fluorescence emission peak at 577 nm. All the measurements were performed under an excitation wavelength of 554 nm and the fluorescence emission scan in the range of 500 - 600 nm.

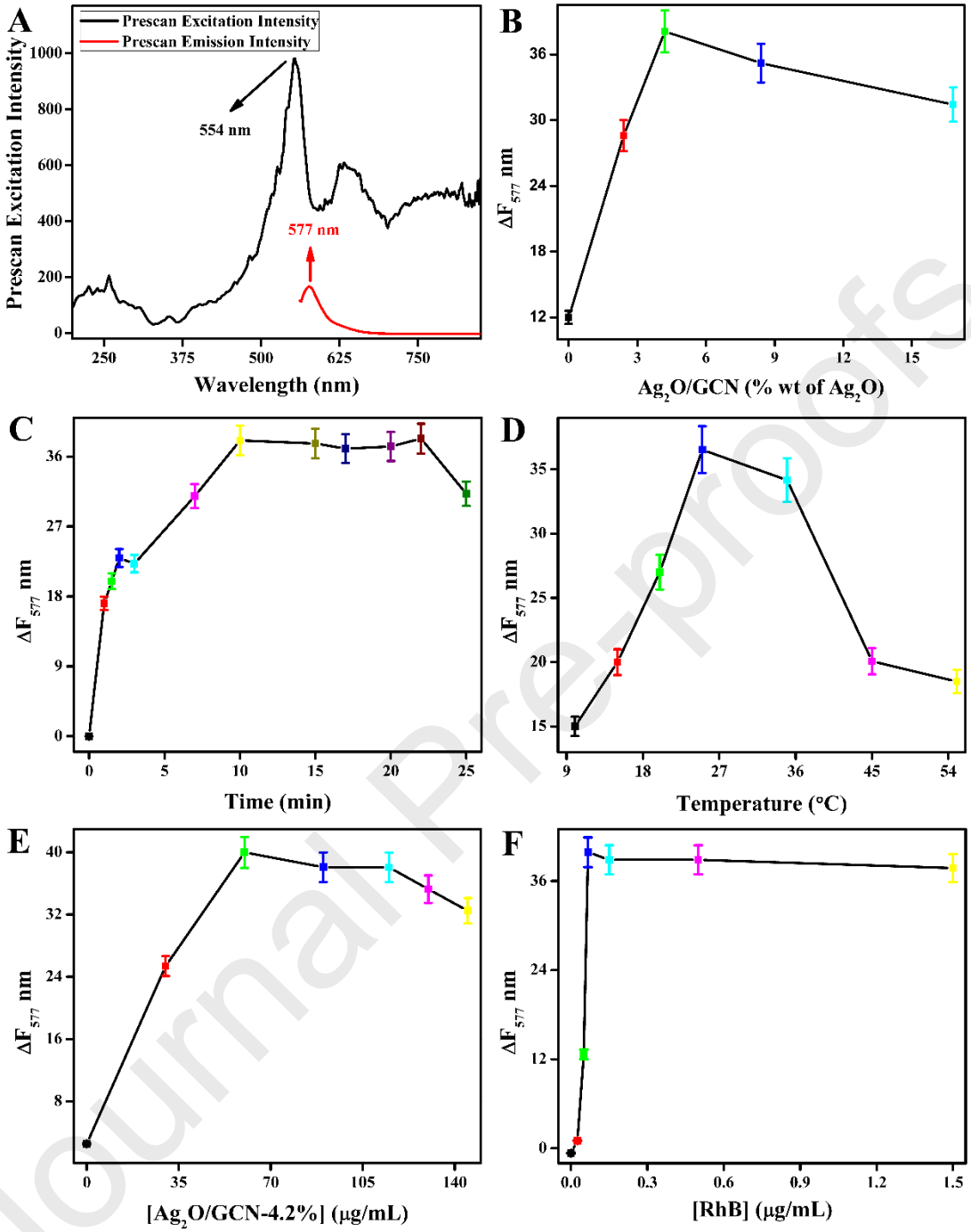

Fig. 10. Pres-scan spectra of RhB solution (A). Optimization of biosensor H_2O_2 detection conditions: Effect of change of Ag_2O percentage (B) time (C) temperature (D) nanocomposite concentration (E) RhB concentration (F) on the fluorescence quenching (ΔF_{557} nm) by H_2O_2. The

reaction condition was 56 μg mL^{-1} of Ag_2O/GCN-4.2% suspension, 66 ng mL^{-1} of RhB, 300 nM of H_2O_2 at room temperature.

The amount of Ag_2O in Ag_2O/GCN nanocomposite was optimized by comparing the catalytic fluorescence quenching response of each synthesized sample. As can be seen in Fig. 10B, that fluorescence quenching was increased as the percentage of Ag_2O was increased from 0 - 4.2 (%), further Ag_2O loading has resulted in a decrease in fluorescence quenching. The RhB-Ag_2O/GCN-4.2% reaction system has shown maximum quenching as compared to the RhB-GCN reaction system because of its high light absorption, large charge transfer, and low electron-hole pairs recombination rate through the junction at the interface of the nanocomposite. Such factors resulted in the high synergistic effect between dye and catalyst. This fluorescence quenching behavior of the nanocomposites could be related to their structural features. It was found that above 4.2 percent loading of Ag_2O, there was an agglomeration of Ag_2O happened and sponge-like structures of GCN were distorted, whereas at 4.2 percent there was a clear, thin, and transparent structure with the large surface area of the nanocomposite. Such morphology supported the presence of more catalytic active sites on the surface of the Ag_2O/GCN-4.2 % nanocomposite as compared to other prepared samples. From these results, the morphological changes and the synergistic effect of Ag_2O nanoparticles and GCN support effected on the superior peroxidase-like catalytic activity. So, Ag_2O/GCN-4.2% nanocomposite was selected for further experimentation on H_2O_2 sensing.

The effect of time on the fluorescence quenching of RhB-Ag_2O/GCN-4.2% reaction system by H_2O_2 was also investigated and shown in Fig. 10C. Results showed that the fluorescence intensity of the system was increased for the first 10 min and then became stable. However, after 10 min of reaction time, the intensity began to reduce. Therefore, the time for the reaction between

RhB-Ag_2O/GCN-4.2% reaction mixture and H_2O_2 was optimized to be 10 minutes. Fig. 10D showed the effect of temperature on the fluorescence quenching efficiency of the prepared H_2O_2 biosensor. The ΔF_{577} nm was dramatically increased as the temperature increased from 0°C to 20°C, which could be explained based on the collision frequency and electrical properties of the semiconductor. At low temperature, collision frequency between RhB-Ag_2O/GCN-4.2%, a fluorescent substance and H_2O_2 was low, which has resulted in a weak fluorescence quenching effect. However, this collision frequency and electrical properties of the catalyst were increased with the increase in temperature, which in turn increased the decomposition of H_2O_2 to form ions and radicals. Hence, oxidation of RhB was increased and an increase in the fluorescence quenching effect was observed. Further, an increase in temperature beyond the room temperature resulted in a decrease in fluorescence quenching. The reason again for this decrease in fluorescence quenching at higher temperatures was the increase in the recombination of the electrical charges phenomenon. This recombination of electrical charges could reduce the efficiency of the catalyst for dye oxidation and hence could reduce the fluorescence quenching effect. The optimum temperature of the nano-catalyst was estimated to be 25°C.

The concentration of Ag_2O/GCN-4.2% nanocomposite directly affected the sensitivity of the biosensor. A low concentration of catalysts led to low sensitivity towards target analyte, however, the extremely high concentration of catalyst has deteriorated the resulting efficiency of the biosensor. Therefore, knowing the optimum concentration of catalyst was paramount important. Fig. 10E showed the effect of concentration of Ag_2O/GCN-4.2% nanocomposite on the H_2O_2 detection. A significant increase in fluorescence quenching was observed as the concentration of catalyst increased from 0 - 58 μg mL^{-1}. Further increase in catalyst concertation has not shown any significant effect on ΔF_{577} nm, which indicated that increasing concentration

of Ag_2O/GCN-4.2% nanocomposite to over 58 μg mL^{-1} has no prominent influence on the detection sensitivity of the biosensor. So, the optimal concentration of Ag_2O/GCN-4.2% nanocomposite suspension was selected to be 58 μg mL^{-1}.

The concentration of RhB also affected the performance of the sensor, and its optimization for designing the sensor was quite important. As shown in Fig. 10F, the fluorescence quenching values of the system was increased with the increase in the concentration of RhB from 0 - 66 ng mL^{-1} at first. Further, the increase in RhB concentration has shown no significant effect on the fluorescence quenching because the reaction system was reached its maximum ΔF_{577} nm value at RhB concentration of 66 ng mL^{-1}. Therefore, the concentration of RhB was optimized as 66 ng mL^{-1} and this concentration of RhB was used for further studies. The optimal conditions of the Ag_2O/GCN-4.2% nanocomposite biosensor for H_2O_2 detection were summarized as follows: reaction temperature of 25°C, the reaction time of 10 min, and the concentration of Ag_2O/GCN-4.2% nanocomposite of 56 μg mL^{-1}. For the convenience of experimentation, all the experiments were performed using PBS (pH 7.2, 10 mM) and at room temperature.

3.4. Fluorescent Quenching Quantitative Detection of H_2O_2

The peroxidase-like catalytic activity of as-prepared GCN and Ag_2O/GCN composites were investigated by using RhB dye as the substrate. In the reaction, Ag_2O/GCN nanocomposites catalyzed the H_2O_2 to produce •OH and then this •OH was assessed by utilizing the fluorescent quenching of RhB.

It was noted during experimentation that the fluorescence signal was emitted only if the RhB was present in the reaction mixture. Further, when H_2O_2 was added in the RhB, the fluorescence of the system was enhanced, which showed that H_2O_2 added a chromophoric effect

to the reaction system. However, when Ag_2O/GCN-4.2% nanocomposite was added in the RhB + H_2O_2 system, the fluorescence intensity was significantly reduced/ quenching (Fig. 11A). This decrease in fluorescence intensity was happened because of the oxidation of RhB to a colorless or non-fluorescent product by •OH radicals and ions produced from H_2O_2 under the catalytic effect of the prepared nanocomposite. Moreover, high catalytic quenching was attributed to high conductivity and enhanced surface area, which aided high adsorption of RhB on the surface area and enhanced photon harvesting ability of Ag_2O/GCN-4.2% nanocomposite. [27] In turn, the recombination rate of photogenerated electrons-holes pairs were suppressed. By assembling Ag_2O and sponge-like GCN, the electrons were transferred from the conduction band of GCN to the conduction band of Ag_2O to adjust fermi energy levels. The recombination time of charge carriers was prolonged due to the separation of charge between charged Ag_2O and charged GCN. At the same time, the fluorescence spectrum of the RhB-Ag_2O/GCN reaction mixture has the identical maximum wavelength and identical fluorescence emission curve shape with that of the spectrum of RhB, which showed that the Ag_2O/GCN could catalyze the H_2O_2 to form •OH and produce a typical fluorescence emission changes. All these findings suggested that the Ag_2O/GCN were found to possessed peroxidase-like activities, which can be applied for the development of the H_2O_2 sensor.

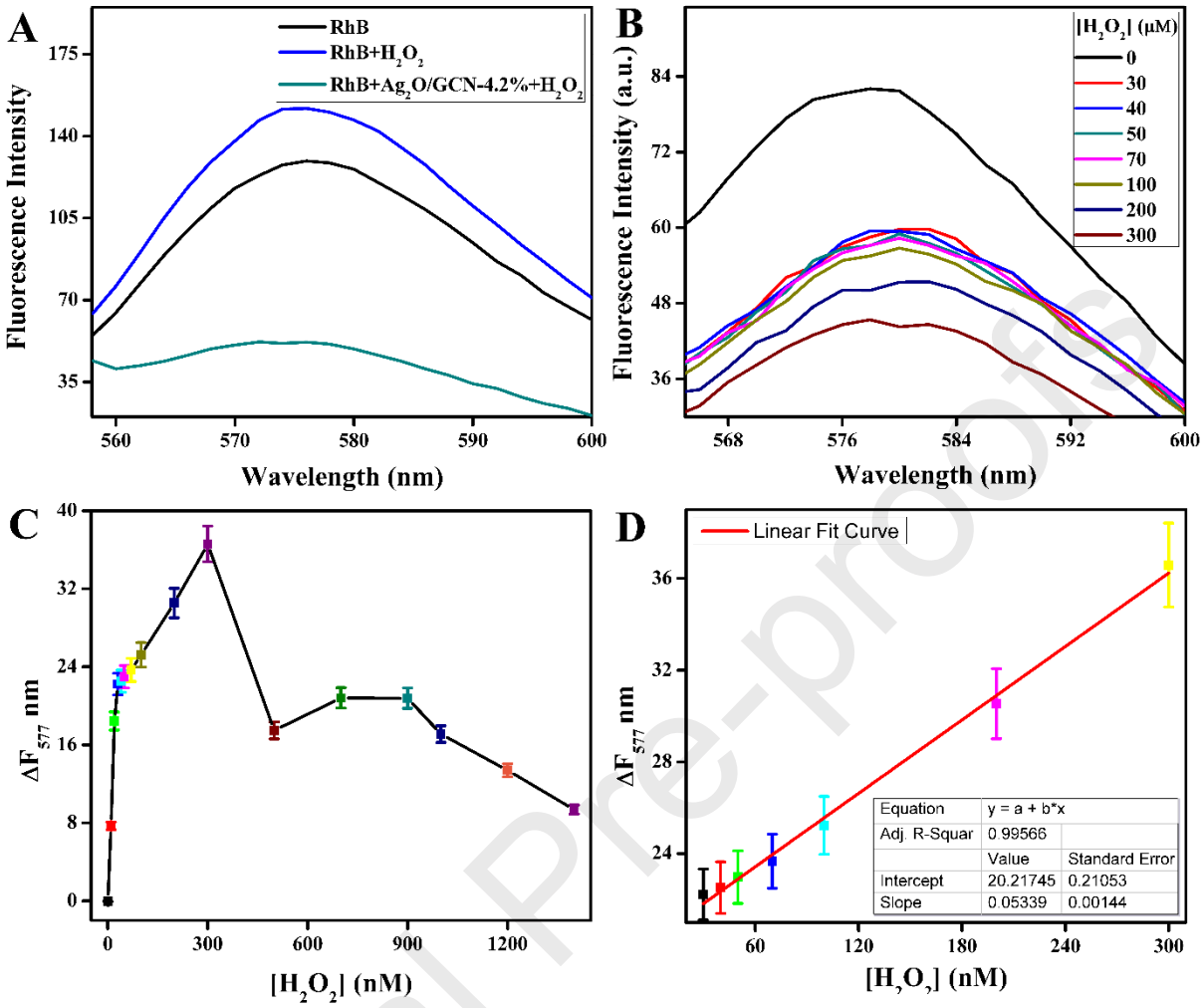

Fig. 11. Comparison of fluorescence emission of RhB in the presence of H_2O_2 and Ag_2O/GCN + H_2O_2 (A), emission spectra of RhB-Ag_2O/GCN-4.2% in the presence of varying concentrations of H_2O_2 (B), relationship between fluorescence quenching at 577 nm and H_2O_2 concentrations (C), calibration curves for the calculation of detection limit (D). The reaction conditions were the same as mentioned in Fig. 10.

Fig. 11B showed the effect of increasing concentration of H_2O_2 on the fluorescence intensity of RhB and Ag_2O/GCN-4.2% reaction system. The fluorescence emission intensity of

the RhB-Ag_2O/GCN-4.2% reaction system at 557 nm was gradually decreased with the increase in H_2O_2 concentration from 0 - 300 nM. To determine and further understand the effect of H_2O_2 concentrations on the fluorescence quenching, ΔF_{577} nm was plotted against the H_2O_2 concentrations from 0 to 1400 nM as shown in Fig. 11C. As can be seen in Fig. 11C that ΔF_{577} nm was increased up to 300 nM of the H_2O_2 concentration. Over this concentration of H_2O_2, ΔF_{577} nm was decreased. This was because of the saturation of H_2O_2 concentration in the reaction mixture. So, 300 nM of H_2O_2 concentration was estimated as equilibrium concentration at which the maximum amount of •OH radicals were produced and the maximum oxidation of RhB molecules took place. Fig. 11D showed that biosensor has an excellent linear relationship with H_2O_2 concentrations in the range of 30 - 300 nM with a linear fitting equation of ΔF_{577} $\text{nm} = 0.05339\text{X} + 20.21745$ ($R^2 = 0.99566$). The limit of detection ($\frac{3.3 \times \sigma}{slop}$ where σ was the standard deviation of the Y-axis) of the developed H_2O_2 biosensor was calculated as 22 nM. Thus, our developed sensor was low cost, simply structured in terms of easier availability.

3.5. UV-Visible Absorption Quantitative Detection of H_2O_2

The UV-Vis absorption spectrum of RhB in PBS was obtained and shown in Fig. 12A. There was a main absorption peak centered at 554 nm for the RhB solution. The addition of Ag_2O/GCN-4.2% nanocomposite in the RhB solution has resulted in the increase of absorption intensity of the main peak at 560 nm as shown in the inset of Fig. 12A. This increase in absorbance intensity can be attributed to the adsorption of RhB on the surface of nanoparticles. As can be seen in Fig. 12B, the addition of H_2O_2 in the RhB-Ag_2O/GCN-4.2% reaction system resulted in a decrease in UV-Vis absorption intensity at 554 nm and catalytic absorption quenching (ΔA_{554} nm) was varied with H_2O_2. This variation was used for the designing of the UV-Vis method for H_2O_2 detection. As shown in Fig. 12C, this decrease remained linear in the range of 30 - 110 nM of the

H_2O_2 concentration. The regression equation of the straight line was $\Delta A_{554}\,\text{nm} = 0.00041338X + 0.09224$ with correlation coefficient (R^2) of 0.99313. The lower limit of detection was calculated as low as 11 nM of H_2O_2 concentration.

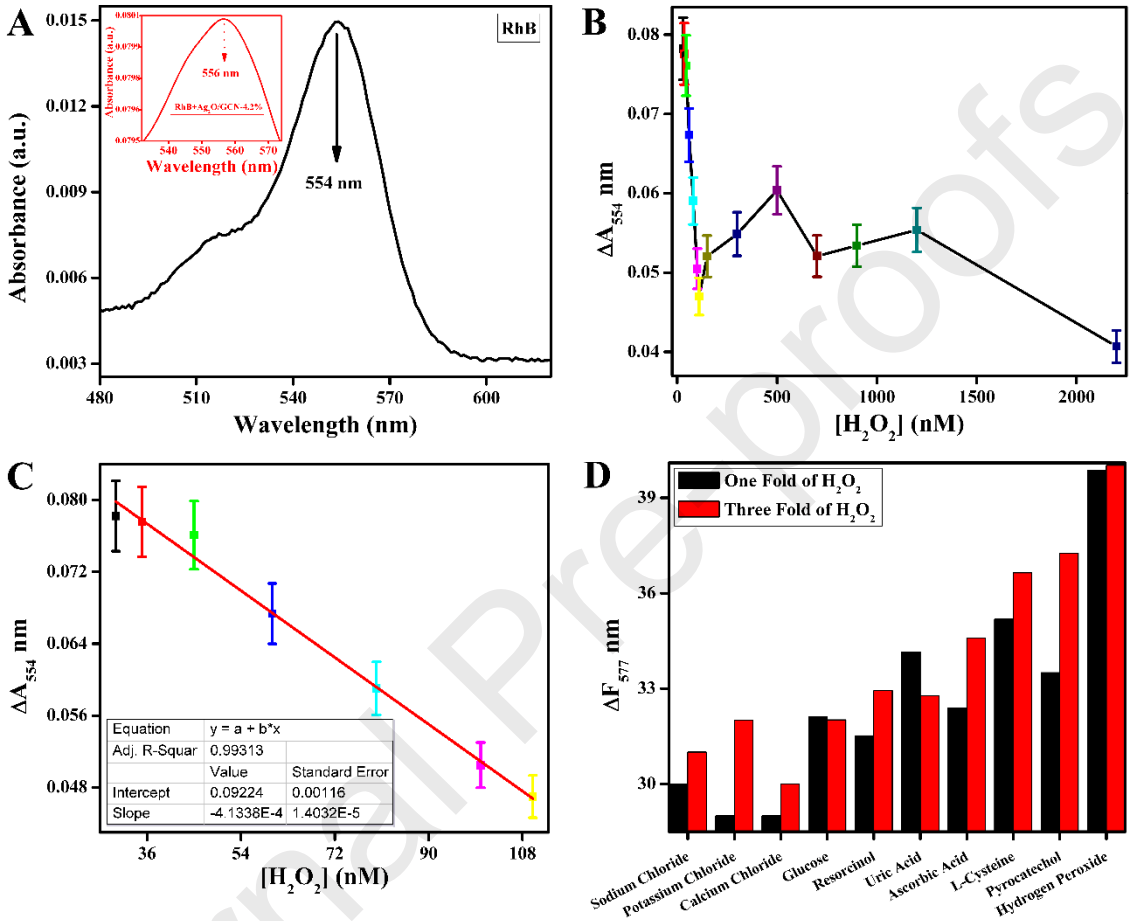

Fig. 12. UV-Vis absorption spectra of RhB in the absence (A) and presence (inset graph of A) of the Ag_2O/GCN-4.2% nanocomposite. Relationship between catalytic absorbance quenching and H_2O_2 concentration (B), a calibration curve of the H_2O_2 detection (C). Histogram for relative catalytic fluorescence quenching of the RhB-Ag_2O/GCN-4.2% reaction system by different target analytes in place of H_2O_2 (D). The reaction conditions were the same as mentioned in Fig. 10.

A comparison of the limit of detections and linear ranges of the reported biosensors constructed through catalytic fluorescence quenching, UV-Vis absorption spectrophotometer

method and the electrochemical method was shown in Table 2. It indicated that the UV-Vis method was not sensitive and possessed a short linear range. Also, our developed biosensor has a much wider linear range as compared to the reported methods.

Table 2. Comparison of the limit of detections and linear ranges obtained from various sensors for H_2O_2 assay.

Materials	**Method**	**Linear Range (nM)**	**LOD (nM)**	**Ref.**
Ag_2O/GCN-4.2%	Fluorescence	30 – 300 ($R^2 = 0.9957$)	22	**Present**
	Colorimetric	30 – 110 ($R^2 = 0.9931$)	11	**Work**
g-C_3N_4	Fluorescence	100 – 2000 × 10^3 ($R^2 = 0.987$)	50	[28]
Ag/porous-g-C_3N_4	Electrochemical	10^5 – 39.5 × 10^6 ($R^2 = 0.999$)	600	[29]
Au NPs/Silica NPs	Luminescence	100-1500	-	[30]
N-acetyl-L-cysteine-Au NCs	Fluorescence	40-4440 ($R^2 = 0.993$)	27	[31]
g-C_3N_4-Fe_3O_4	Colorimetric	10^6 – 40 × 10^6 ($R^2 = 0.9948$)	300	[32]

3.6. The selectivity of the Sensor

Besides sensitivity, selectivity is another important parameter to find the performance of a sensor. Therefore, to investigate the selectivity of H_2O_2 biosensor, catalytic fluorescence quenching of RhB-Ag_2O/GCN-4.2% reaction system by different potential interfering analytes like sodium chloride, potassium chloride, calcium chloride, glucose, resorcinol, uric acid, ascorbic

acid, L-cysteine and pyrocatechol was studied. The reaction mixture was contained 56 μg mL^{-1} of the Ag_2O/GCN-4.2% nanocomposite, 66 ng mL^{-1} of the RhB and 300 nM of the analyte of interest at room temperature in PBS (pH 7.2, 10 mM). As shown in Fig. 12D, the catalytic fluorescence quenching response by all species was less than the catalytic fluorescence quenching response of H_2O_2 under identical experimental conditions. These results indicated that the catalytic fluorescence quenching method was more selective to the determination of H_2O_2 as compared to other oxidants. Thus, our fabricated non-enzymatic sensor of Ag_2O/GCN-4.2% nanocomposite has demonstrated high selectivity, good reliability, and anti-interference property for the detection of H_2O_2.

4. CONCLUSIONS

In summary, sponge-like GCN was successfully synthesized from melamine by calcination method and Ag_2O/GCN nanocomposites were synthesized from bulk sponge-like GCN, $AgNO_3$ and K_2HPO_4 by hydrothermal method. The prepared nanocomposite samples also exhibited a sponge-like structure. Due to the randomly interconnecting and weak van der Waal interaction among nanosheets in sponge structure, the ultrasonication method was used to prepare the suspension of the synthesized samples and these suspensions were employed to determine the peroxidase-like-catalytic-activity for the reaction between RhB and H_2O_2. Prepared nanocomposites were characterized by different analytical techniques to understand the structure and activity relationship. Obtained characterization results showed a decrease in the bandgap for carbon nitride after the addition of silver oxide. Furthermore, the loading of silver oxide in carbon nitride reduced the recombination of electron holes pairs and resulted in the increase of sensitivity of the prepared system for H_2O_2 detection. Optimization of different parameters such as temperature, pH, time, the concentration of fluorescent dye, concentration of nanocomposite and

H_2O_2 was performed to get a deep insight into the working of the system. The detection of H_2O_2 was observed through the extent of catalytic fluorescence quenching of dye in the presence of prepared samples as catalyst and H_2O_2. The developed fluorescence probe has shown high selectivity and sensitivity towards H_2O_2 detection with a linear range of 30 - 300 nM and a detection limit of 22 nM. Ease of production, rapid detection, superior selectivity, high sensitivity and lower limit of detection were the advantages of the proposed catalytic fluorescence quenching biosensor. This developed biosensor has a lot of potential in the chemical, biological and environmental biosensing applications.

ACKNOWLEDGEMENT:

This work was supported by the Higher Education Commission Pakistan through its NRPU grant 20-4993/R&D/HEC/14 and Pakistan Science Foundation through its PSF-NSFC funded project (Project No. PSF/NSFC-II/Eng/P-COMSATS-Lhr(07).

CONFLICTS OF INTEREST: The authors declare no conflict of interest.

REFERENCES

[1] N.K. Sekar, M.B. Gumpu, B.L. Ramachandra, N. Nesakumar, P. Sankar, K.J. Babu, U.M. Krishnan, J.B.B. Rayappan, Fabrication of Electrochemical Biosensor with ZnO-PVA Nanocomposite Interface for the Detection of Hydrogen Peroxide, Journal of nanoscience and nanotechnology, 18 (2018) 4371-4379.

[2] W. Liu, K. Hiekel, R. Hübner, H. Sun, A. Ferancova, M. Sillanpää, Pt and Au bimetallic and monometallic nanostructured amperometric sensors for direct detection of hydrogen peroxide: influences of bimetallic effect and silica support, Sensors and Actuators B: Chemical, 255 (2018) 1325-1334.

[3] B.E. Watt, A.T. Proudfoot, J.A. Vale, Hydrogen peroxide poisoning, Toxicological reviews, 23 (2004) 51-57.

[4] J.S. Kumar, N.C. Murmu, P. Samanta, A. Banerjee, R.S. Ganesh, H. Inokawa, T. Kuila, Novel synthesis of a Cu 2 O–graphene nanoplatelet composite through a two-step electrodeposition method for selective detection of hydrogen peroxide, New Journal of Chemistry, 42 (2018) 3574-3581.

[5] X. Cui, S. Wu, Y. Li, G. Wan, Sensing hydrogen peroxide using a glassy carbon electrode modified with in-situ electrodeposited platinum-gold bimetallic nanoclusters on a graphene surface, Microchimica Acta, 182 (2015) 265-272.

[6] S. Chen, R. Yuan, Y. Chai, F. Hu, Electrochemical sensing of hydrogen peroxide using metal nanoparticles: a review, Microchimica Acta, 180 (2013) 15-32.

[7] A. Farooq, R. Al-Jowder, R. Narayanaswamy, M. Azzawi, P.J.R. Roche, D.E. Whitehead, Gas detection using quenching fluorescence of dye-immobilised silica nanoparticles, Sensors and Actuators B: Chemical, 183 (2013) 230-238.

[8] G. Tang, L. Du, X. Su, Detection of melamine based on the fluorescence resonance energy transfer between CdTe QDs and Rhodamine B, Food Chem, 141 (2013) 4060-4065.

[9] A. Sakuragawa, T. Taniai, T. Okutani, Fluorometric determination of microamounts of hydrogen peroxide with an immobilized enzyme prepared by coupling horseradish peroxidase to chitosan beads, Analytica Chimica Acta, 374 (1998) 191-200.

[10] H.-B. Fang, Y. Luo, Y.-Z. Zheng, W. Ma, X. Tao, Facile Large-Scale Synthesis of Urea-Derived Porous Graphitic Carbon Nitride with Extraordinary Visible-Light Spectrum Photodegradation, Industrial & Engineering Chemistry Research, 55 (2016) 4506-4514.

[11] Z. Zhou, Y. Zhang, Y. Shen, S. Liu, Y. Zhang, Molecular engineering of polymeric carbon nitride: advancing applications from photocatalysis to biosensing and more, Chem Soc Rev, 47 (2018) 2298-2321.

[12] L. Shi, L. Liang, J. Ma, F. Wang, J. Sun, Enhanced photocatalytic activity over the Ag2O–g-C3N4 composite under visible light, Catalysis Science & Technology, 4 (2014) 758.

[13] B. Long, J. Lin, X. Wang, Thermally-induced desulfurization and conversion of guanidine thiocyanate into graphitic carbon nitride catalysts for hydrogen photosynthesis, Journal of Materials Chemistry A, 2 (2014) 2942.

[14] W. Lu, J. Shu, Z. Wang, N. Huang, W. Song, The intrinsic oxidase-like activity of Ag2O nanoparticles and its application for colorimetric detection of sulfite, Materials Letters, 154 (2015) 33-36.

[15] A. Allahresani, M.A. Nasseri, A. Nakhaei, SiO2/g-C3N4 nanocomposite-catalyzed green synthesis of di-indolyloxindols under mild conditions, Research on Chemical Intermediates, 43 (2017) 6367-6378.

[16] N. Cheng, J. Tian, Q. Liu, C. Ge, A.H. Qusti, A.M. Asiri, A.O. Al-Youbi, X. Sun, Au-nanoparticle-loaded graphitic carbon nitride nanosheets: green photocatalytic synthesis and application toward the degradation of organic pollutants, ACS applied materials & interfaces, 5 (2013) 6815-6819.

[17] A. Akhundi, A. Habibi-Yangjeh, A simple large-scale method for preparation of g-C3N4/SnO2 nanocomposite as visible-light-driven photocatalyst for degradation of an organic pollutant, Materials Express, 5 (2015) 309-318.

[18] P. Niu, L. Zhang, G. Liu, H.-M. Cheng, Graphene-Like Carbon Nitride Nanosheets for Improved Photocatalytic Activities, Advanced Functional Materials, 22 (2012) 4763-4770.

[19] S. Liang, D. Zhang, X. Pu, X. Yao, R. Han, J. Yin, X. Ren, A novel Ag2O/g-C3N4 p-n heterojunction photocatalysts with enhanced visible and near-infrared light activity, Separation and Purification Technology, 210 (2019) 786-797.

[20] X. Wang, J. Yan, H. Ji, Z. Chen, Y. Xu, L. Huang, Q. Zhang, Y. Song, H. Xu, H. Li, MO degradation by Ag-Ag2O/g-C3N4 composites under visible-light irradiation, Springerplus, 5 (2016) 369.

[21] M. Xu, L. Han, S. Dong, Facile fabrication of highly efficient g-C3N4/Ag2O heterostructured photocatalysts with enhanced visible-light photocatalytic activity, ACS Appl Mater Interfaces, 5 (2013) 12533-12540.

[22] H.-T. Ren, S.-Y. Jia, Y. Wu, S.-H. Wu, T.-H. Zhang, X. Han, Improved Photochemical Reactivities of Ag2O/g-C3N4 in Phenol Degradation under UV and Visible Light, Industrial & Engineering Chemistry Research, 53 (2014) 17645-17653.

[23] Z. Jiang, S. Le, Y. Xie, Q. Huang, B. Wang, T. Jiang, mpg-C3N4/Ag2O Nanocomposites Photocatalysts with Enhanced Visible-Light Photocatalytic Performance, Journal of Nanoscience and Nanotechnology, 19 (2019) 721-728.

[24] J. Fu, Y. Tian, B. Chang, F. Xi, X. Dong, BiOBr–carbon nitride heterojunctions: synthesis, enhanced activity and photocatalytic mechanism, Journal of Materials Chemistry, 22 (2012) 21159.

[25] W.-J. Ong, L.K. Putri, Y.-C. Tan, L.-L. Tan, N. Li, Y.H. Ng, X. Wen, S.-P. Chai, Unravelling charge carrier dynamics in protonated g-C3N4 interfaced with carbon nanodots as co-catalysts toward enhanced photocatalytic CO2 reduction: A combined experimental and first-principles DFT study, Nano Research, 10 (2017) 1673-1696.

[26] Z. Jiang, C. Zhu, W. Wan, K. Qian, J. Xie, Constructing graphite-like carbon nitride modified hierarchical yolk-shell TiO2 spheres for water pollution treatment and hydrogen production, Journal of Materials Chemistry A, 4 (2016) 1806-1818.

[27] G. Rezanejade Bardajee, Z. Hooshyar, M. Khanjari, Dye fluorescence quenching by newly synthesized silver nanoparticles, Journal of Photochemistry and Photobiology A: Chemistry, 276 (2014) 113-121.

[28] J.W. Liu, Y. Luo, Y.M. Wang, L.Y. Duan, J.H. Jiang, R.Q. Yu, Graphitic Carbon Nitride Nanosheets-Based Ratiometric Fluorescent Probe for Highly Sensitive Detection of H2O2 and Glucose, ACS Appl Mater Interfaces, 8 (2016) 33439-33445.

[29] D. Jiang, Y. Zhang, H. Chu, J. Liu, J. Wan, M. Chen, N-doped graphene quantum dots as an effective photocatalyst for the photochemical synthesis of silver deposited porous graphitic C3N4 nanocomposites for nonenzymatic electrochemical H2O2 sensing, RSC Advances, 4 (2014) 16163-16171.

[30] N.A. Burmistrova, O.A. Kolontaeva, A. Duerkop, New Nanomaterials and Luminescent Optical Sensors for Detection of Hydrogen Peroxide, Chemosensors, 3 (2015) 253-273.

[31] H.-H. Deng, G.-W. Wu, D. He, H.-P. Peng, A.-L. Liu, X.-H. Xia, W. Chen, Fenton reaction-mediated fluorescence quenching of N-acetyl-l-cysteine-protected gold nanoclusters: analytical applications of hydrogen peroxide, glucose, and catalase detection, Analyst, 140 (2015) 7650-7656.

[32] J. Chen, Q. Chen, J. Chen, H. Qiu, Magnetic carbon nitride nanocomposites as enhanced peroxidase mimetics for use in colorimetric bioassays, and their application to the determination of H2O2 and glucose, Microchimica Acta, 183 (2016) 3191-3199.

TOC Graphics

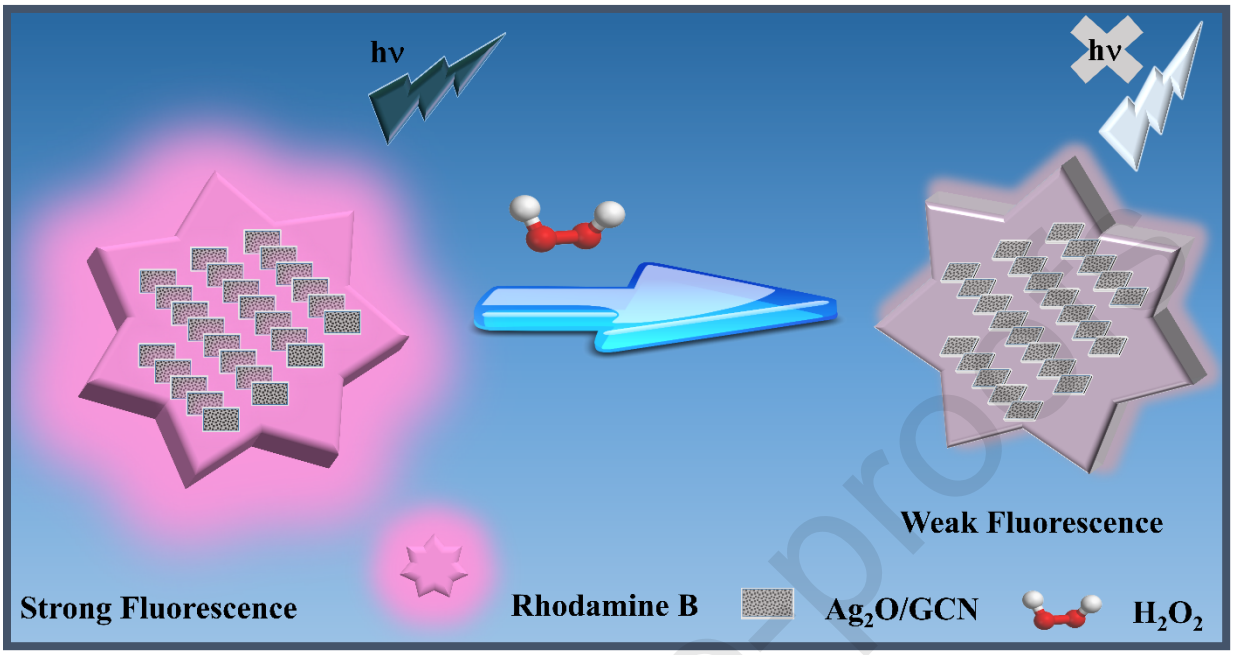

HIGHLIGHTS

- Fabrication of Sponge-like hierarchical g-C_3N_4 and Ag_2O nanocomposites.
- Improved electrical properties through the synergistic effect of g-C_3N_4 and Ag_2O.
- Highly sensitive and selective fluorescence quenching method for H_2O_2 detection.